Multi-filter Photometric Analysis of W Ursae Majoris (W UMa) Type Eclipsing Binary Stars KID 11405559 and V342 Boo

Tatsuya Akiba
University of Colorado Boulder, Department of Astrophysical and Planetary Sciences, 2000 Colorado Ave, Duane Physics Building, Rm. E226, Boulder, CO 80309; address email correspondence to gokhale@truman.edu

Andrew Neugarten
Subaru Telescope, National Astronomical Observatory of Japan, 650 North A'ohōkū Place, Hilo, HI 96720

Charlyn Ortmann
Vayujeet Gokhale
Truman State University, 100 E. Normal Street, Kirksville, MO 63501; gokhale@truman.edu

Received July 30, 2019; revised October 2, November 4, 2019; accepted November 12, 2019

Abstract We present light curve analysis of two variable stars, KID 11405559 and V342 Boo. KID 11405559 is selected from the Kepler Eclipsing Binary Catalog published by Kirk *et al.* (2016) and V342 Boo from a list of eclipsing binaries published by Kreiner (2004). In this paper, we present the light curves for these two objects using data collected at the 31-inch NURO telescope at Lowell Observatory in Flagstaff, Arizona, in three filters: Bessell B, V, and R. We generate truncated twelve-term Fourier fits for the light curves and quantify the O'Connell effect exhibited by these systems by calculating the difference ΔI in the heights of the primary and secondary maxima: the "Light Curve Asymmetry" (LCA) and the "O'Connell Effect Ratio" (OER). Additionally, we use the Fourier coefficients from the Fourier fit to confirm that KID 11405559 and V342 Boo are W UMa type eclipsing binary stars.

1. Introduction

The O'Connell Effect is the inequality in the out-of-eclipse maxima in the light curve of eclipsing binaries (O'Connell (1951). This inequality is unexpected, since one expects to receive the same amount of light from each of the components of the binary when the components are side-by-side, irrespective of which component is on which side. Several explanations have been proposed to explain the origin of this effect, but none of these theories are widely applicable to the systems exhibiting the O'Connell effect (see Wilsey and Beaky (2009)). The two models that have received attention recently are the "starspot" model and the "hotspot" model. The former model is based on introducing one or more starspots (regions cooler than the rest of the photosphere) on one, or both, components. The "hotspot" model is applicable for mass-transferring systems where the mass transfer impacts the accretion disk around the accreting star, resulting in an asymmetry in the luminosity of the binary system as viewed from Earth. Again, neither of these models is satisfactory—the "starspot" model essentially introduces an arbitrary number of free parameters with minimal, if any, constraints. Consequently, by adding any number of starspots of varying sizes, shapes, and temperatures it should be possible to fit any light curve. Also, the O'Connell effect has been observed in detached, over-contact, and semi-detached systems and so at best, the `hotspot' model can only work for a certain class of systems exhibiting the O'Connell effect.

Eclipsing binary systems are classified into three main categories, based on the shape and variations in the observed light curves. Of the three types, W UMa-type systems are of particular interest to us since their structure and evolution are still not completely understood. Their light curves are characterized by continuous variability and similar depths of the two minima, caused by the ellipsoidal nature and the proximity of the two components. These systems are to be distinguished from β-Lyrae-type systems which display continuous variability but different depths of the minima, and Algol-type systems which exhibit a nearly constant brightness outside of eclipses. Algols and β-Lyraes are usually considered to be detached and semi-detached systems, respectively, whereas W UMa systems are considered near or over-contact systems. The continuously varying, smooth light curves of W UMa systems are ideal for Fourier analysis.

In this paper, we discuss light curve analysis of two eclipsing binary systems selected from Kirk *et al.* (2016) and Kreiner (2004), namely KID 11405559 and V342 Boo. Firstly, we use the criteria set by Rucinski (1997) to classify these systems as either Algol, β-Lyrae, or W UMa-type systems. We focus on the asymmetries in the light curves in each of the filters by calculating the difference in the heights of the primary and secondary maxima (ΔI), the "Light Curve Asymmetry" (LCA), and the"O'Connell Effect Ratio" (OER). The OER and LCA provide insight into the asymmetries of the light curve regions between the two eclipses (McCartney 1999). The OER is the ratio of the area under the curves between phases $\Phi = 0.0$ to $\Phi = 0.5$ and phases $\Phi = 0.5$ to $\Phi = 1.0$ (see section 3 below). An OER > 1 implies that the first half of the light curve has more total flux than the second half. The LCA, on the other hand, measures the deviance from symmetry of the two halves of the light curve. If both halves are perfectly symmetric, then we would expect the LCA to be zero. Note that the LCA and OER quantify different aspects of the O'Connell effect. For example, an OER equal to 1 does not necessarily imply an LCA equal to 0. The reason for this is that one can imagine

a light curve with a tall but narrow peak maximum and short but wide secondary maximum. Although the areas under the curve of each region may be equal, the curves would be very asymmetric (Gardner 2015).

This project is part of an ongoing effort at Truman State University to introduce undergraduate students to differential aperture photometry by following several eclipsing binary systems per semester with the aim of generating and analyzing their light curves. As mentioned, we are focused on quantifying the asymmetries in the light curves and modeling the systems. System modeling is challenging without having spectroscopic data, since photometric data alone are not enough to constrain the system and determine a unique solution (Prša 2018). Consequently, we do not attempt to model the systems under consideration. However, we demonstrate that by superposing the two halves of an appropriately phased light curve, one can identify the phase at which the light curves are asymmetric (see section 3). In the starspot model, this phase information can be used to constrain the location and characteristics of the starspots. This information can be invaluable in testing the starspot model for EBs using high quality data over hundreds or thousands of orbital cycles —the kind of data we have access to from the Kepler (Prša 2011) and Transiting Exoplanet Survey Satellite (TESS) missions (Ricker *et al.* 2015). Indeed, our group is currently studying how the asymmetry in the light curve evolves over hundreds of orbits for several Kepler EBs (Koogler *et al.* 2019).

The outline of this paper is as follows: In the following section, we outline our observational data acquisition and data reduction methods, followed by an analysis of the light curves in section 3. We conclude in section 4 with a discussion on our results and our future plans.

2. Observations

We present BVR photometry of eclipsing variable stars KID 11405559 ($P = 0.284941$ d) and V342 Boo ($P = 0.29936$ d). The data were collected using the 2k × 2k Loral NASACam CCD attached to the 31-inch National Undergraduate Research Observatory (NURO) telescope at Lowell Observatory, Flagstaff, Arizona (Table 1). The filters used are Bessell BVR. The images are processed by bias subtraction and (sky) flat fielding using the software package MAXIM DL (Diffraction Limited 2012). No dark subtraction was performed since for the nitrogen-cooled camera at NURO, the dark current is negligible. Differential photometry is then performed on the target with a suitable comparison and check star, using MAXIM DL. The aperture size was adjusted to match between 3 to 4 times the full width at half maximum (FWHM) of the brightest object on which photometry was performed for a given target. Similarly, the inner sky annulus was adjusted to about 5 times the FWHM. We searched for any comparison stars from the Tycho (Høg *et al.* 2000) and the American Association of Variable Star Observers (AAVSO) Photometric All-Sky Survey (APASS; Henden *et al.* 2016) catalogues that are present in the image frame, and used these stars to determine the *B* and *V* magnitudes of each of the targets (Table 2). Instrumental magnitudes were used for the *R*-filter since the *R* magnitudes for comparison and check stars were not listed. Stars of brightness comparable to the target star were chosen as check stars. We inspected and confirmed that the check and comparison stars show no variability in each of the filters for both objects. The error on a single observation in each of the filters was approximately 2 mmag for both objects.

Table 1. Observation dates, instrument, and filters for the targets.

Target	*Date of Observation*	*Telescope*	*Filters*
KID 11405559	05/21/2017	NURO	Bessell BVR
	05/22/2017	NURO	Bessell BVR
	05/23/2017	NURO	Bessell BVR
	05/24/2017	NURO	Bessell BVR
V342 Boo	05/21/2017	NURO	Bessell BVR
	05/22/2017	NURO	Bessell BVR

3. Analysis and results

3.1. Light curves

To plot a light curve, the time axis is phase-folded using the equation

$$\Phi = \frac{T - T_0}{P} - \text{Int}\left(\frac{T - T_0}{P}\right) \quad (1)$$

where T is the time, P is the period of the object, and T_0 is an arbitrary epoch. The resulting light curves for each object in the B and V filters are shown in Figure 1. Only the B and V plots are shown since we could not identify a star with a reliable R magnitude in the image field. We calculate and set the epoch of the primary minimum, defined as the deeper of the two eclipses, as phase "0". This is achieved by setting the epoch, T_0 in Equation 1 to the epoch of the primary minimum.

In the B and V light curves, we see that the two systems have similar but slightly different depths of minima. The light curves for both objects are smoothly varying with comparable primary and secondary minima characteristic of W UMa systems.

Table 2. Target, comparison, and check star coordinates, and comparison star B and V magnitudes.

Star	*Name*	*R.A. (J2000)* h m s	*Dec. (J2000)* ° ′ ″	*V*	*B*
Target	KID 11405559	19 32 54.16	+49 14 33.2		
Comparison	KID 11352756	19 33 20.82	+49 17 54.4	11.22	12.41
Check	TYC 3564-1900-1	19 32 19.00	+49 10 47.7	11.67	14.07
Target	V342 Boo	13 59 53.52	+17 53 57.4		
Comparison	—	13 59 35.81	+17 50 42.8	13.116	13.724
Check	—	13 59 57.98	+17 56 48.0	13.777	14.92

A modest O'Connell effect is seen as well, with the secondary maxima (the maxima following the secondary eclipse) slightly higher than the primary maxima. This effect is even more prominent when the normalized flux is plotted, instead of the magnitude (see Figure 2). For each data point, the normalized flux (Warner and Harris 2006) is calculated from the magnitude by applying the equation

$$I(\Phi)_{\text{obs}} = 10^{-0.4 \times (m(\Phi) - m(\max))} \quad (2)$$

where $m(\Phi)$ is the magnitude at a certain phase Φ and $m(\max)$ is the maximum magnitude observed for the object. We perform Fourier fit analyses on the light curves of each object in each filter similar to Wilsey and Beaky (2009). A truncated twelve-term Fourier fit is given by

$$I(\Phi)_{\text{fit}} = a_0 + \sum_{n=1}^{12} (a_n \cos(2\pi n\Phi) + b_n \sin(2\pi n\Phi)) \quad (3)$$

where a_0, a_n, and b_n are the Fourier coefficients of the fit, and Φ is the phase (Hoffman *et al.* 2009). Note that the Fourier fits are generated after the data are adjusted to align the primary eclipse with phase "0". The light curves of the two objects in each filter along with their Fourier fits are presented in Figure 2.

We use the phased normalized flux plots (Figure 2) and the corresponding Fourier fits to classify the two systems, and then proceed to discuss the asymmetries in the light curve.

3.2. Classification of systems

In this paper, we apply the following criteria to classify the systems:

1. Distinguish the systems as either W UMa or β-Lyrae, or detached Algol type systems utilizing Rucinski's (1997) criterion:

   (a) if $a_4 > a_2\,(0.125 - a_2)$ then the system can be considered a W UMa or a β-Lyrae system.

   (b) if $a_4 < a_2\,(0.125 - a_2)$ then the system may be considered a detached eclipsing binary or an Algol.

   Note that both coefficients a_2 and a_4 are negative.

2. If condition (a) above is met, use the Fourier coefficient a_1 to distinguish between a W UMa or β-Lyrae system as follows Wilsey and Beaky (2009):

   (a) if $|a_1| < 0.05$ the system is classified as a W UMa type

   (b) if $|a_1| > 0.05$ the system is of the β-Lyrae type.

Rucinski (1973, 1993, 1997) provides an excellent overview of the use of the Fourier coefficients in determining the orbital elements of eclipsing binary stars. As discussed in Gardner *et al.* (2015), a_2 is a measure of the global distortion of the contact structure, whilst a_4 represents the more localized eclipse effects. On the other hand, the first cosine term from the Fourier fit (a_1) is the dominant term contributing to the difference in the primary and secondary eclipse magnitudes (Wilsey and Beaky 2009). Hence, the first cosine coefficient a_1 provides a measure

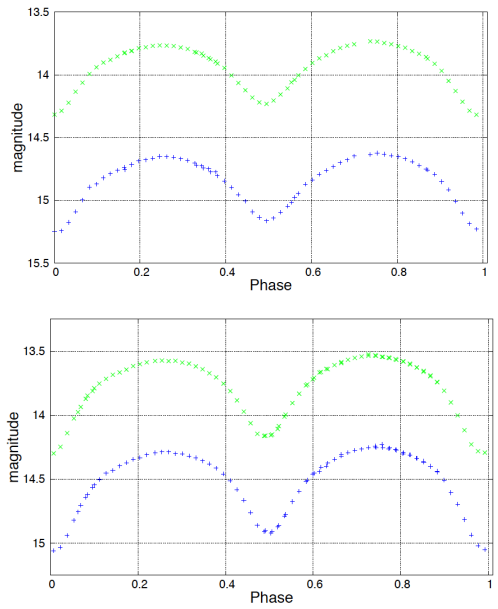

Figure 1. Light curves for KID 11405559 (upper plot) and V342 Boo (lower plot) in the B and V filters (blue and green, respectively). Note the depth of the primary and secondary minima is comparable—a distinctive characteristic of W UMa type systems. The average error on each measurement for both objects in each filter is 0.002 magnitude. Error bars are not shown for the sake of clarity.

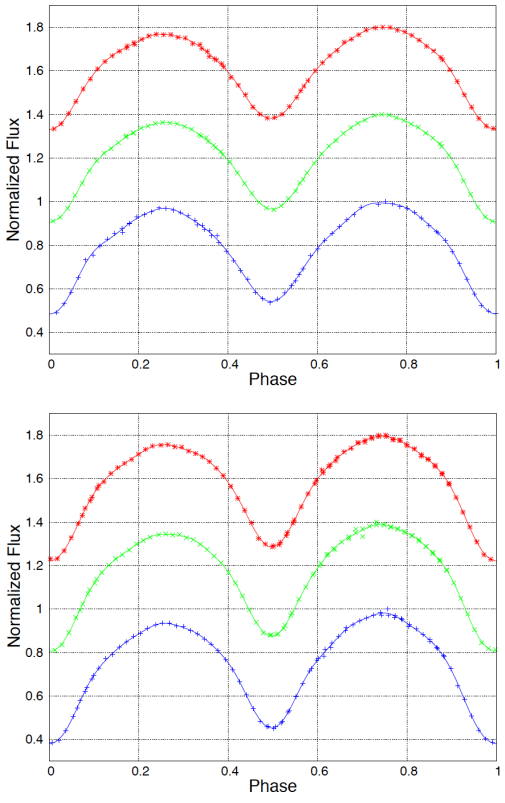

Figure 2. Normalized flux for KID 11405559 (upper plot) and V342 Boo (lower plot). The Fourier fits (continuous curves) are plotted along with the blue, green, and red curves corresponding to B, V, and R filters, respectively. The average error in the flux for each measurement for both objects in each filter is 0.001. Error bars are not shown for the sake of clarity.

of the magnitude difference of the two eclipses and is given by $-2a_1$. We experimented with our Fourier fit coefficients to determine that if the depth of the primary and secondary minima are exactly equal, then a_1 is identically zero. With increasing a_1, the difference between the magnitudes of the two eclipses becomes more prominent, which can be used to distinguish a W UMa system from a β-Lyrae system. When criterion (1a) above is clearly satisfied, and when $|a_1| \approx 0.05$, the depths of the minima differ by approximately 10%, which we take as the dividing line between a W UMa and a β-Lyrae type system.

We evaluated these relationships for each of our objects and the results are recorded in Table 3. The uncertainties of the Fourier coefficients are determined using the NonlinearModelFit function (Wolfram Res. Co. 2019) on MATHEMATICA, where each data point was weighted by the square of its signal-to-noise ratio (SNR).

3.3. Asymmetries in the light curve: quantifying the O'Connell Effect

The simplest way to quantify the O'Connell effect is to calculate the difference in the normalized flux near the primary (I_p) and secondary (I_s) maxima:

$$\Delta I \equiv I_p - I_s$$

A positive ΔI implies that the peak after the primary eclipse is brighter than the peak after the secondary eclipse. A negative ΔI implies the opposite.

We calculate ΔI in two ways:

1. Firstly, we found the values of the two peak magnitudes of the Fourier fit functions. The difference between the two maxima gives us a measure of the the O'Connell effect. These values are presented in Table 4 as "ΔI (Fourier)."

$$\Delta I_{\text{fit}} = I_{p\text{fit}} - I_{s\text{fit}} \quad (4)$$

2. Secondly, all of the data points within ± 0.05 phase of each maximum are averaged. The difference between the two average values for the maxima is calculated, yielding another measure of ΔI. These values are recorded in Table 4 as "ΔI (Average)."

$$\Delta I_{\text{Ave}} = \langle I_p \rangle - \langle I_s \rangle \quad (5)$$

In both systems, and in all filters, both methods result in a negative ΔI (Table 4), which is consistent with Figure 2.

Table 4. Quantifying the O'Connell Effect in terms of difference in maxima. Please see the text (section 3.3) for details.

Target	*Filter*	$\lvert 2b_1 \rvert$	ΔI *(Fourier)*	ΔI *(Average)*
KID 11405559	B	0.032 ± 0.003	-0.024 ± 0.008	-0.029 ± 0.002
	V	0.031 ± 0.001	-0.036 ± 0.004	-0.0321 ± 0.0008
	R	0.029 ± 0.002	-0.031 ± 0.005	-0.035 ± 0.002
V342 Boo	B	0.041 ± 0.002	-0.044 ± 0.005	-0.045 ± 0.002
	V	0.040 ± 0.002	-0.044 ± 0.006	-0.040 ± 0.005
	R	0.036 ± 0.002	-0.038 ± 0.005	-0.0373 ± 0.0007

The first sine term in the Fourier series has extrema at phase Φ = 0.25 and Φ = 0.75, the locations of the out-of-eclipse maxima in the light curves. This makes it the dominant component accounting for the asymmetry in the peak magnitudes (Wilsey and Beakey 2009, Gardner *et al.* 2015). The coefficient, b_1, associated with the first sine term is the half-amplitude of the sine wave and consequently, $|2b_1|$ is a good approximation to ΔI. The calculated values of $|2b_1|$, ΔI (Fourier) and ΔI (Average) are shown in Table 4. The uncertainties for $|2b_1|$ and ΔI_{fit} are calculated by propagating the uncertainties on the Fourier coefficients (See Appendices B and C). Note that the uncertainty on ΔI_{Ave} is calculated from the addition of uncertainties in quadrature of the data points used in the average (Appendix C), and consequently is a function of the signal-to-noise ratio (i.e. how good our data are) close to the two maxima. This leads to significant variation in the errors on ΔI_{Ave}.

We also quantified the O'Connell effect by calculating the O'Connell Effect Ratio (OER) and the "Light Curve Asymmetry" (LCA) as described by McCartney (1999). As mentioned, The OER is simply the ratio of the area under the curves between phases Φ = 0.0 to Φ = 0.5 and phases Φ = 0.5 to Φ = 1.0, whilst the LCA measures the deviance from symmetry of the two halves of the light curve. The OER and LCA are given by:

$$\text{OER} = \frac{\int_{0.0}^{0.5} (I(\Phi)_{\text{fit}} - I(\Phi)_{\text{fit}}) d\Phi}{\int_{0.5}^{1.0} (I(\Phi)_{\text{fit}} - I(\Phi)_{\text{fit}}) d\Phi} \quad (6)$$

And

$$\text{LCA} = \sqrt{\int_{0.0}^{0.5} \frac{(I(\Phi)_{\text{fit}} - I(1.0-\Phi)_{\text{fit}})^2}{I(\Phi)^2_{\text{fit}}} d\Phi} \quad (7)$$

where, $I(\Phi)_{\text{fit}}$ is given by Equation 3. The values for these parameters are tabulated in Table 5. The uncertainties of the

Table 3. Classification of systems based on Fourier coefficients.

Target	*Filter*	a_1	a_2	a_4	$a_2(0.125 - a_2)$	*Classification*
KID 11405559	B	0.015 ± 0.001	–0.218 ± 0.001	–0.0426 ± 0.0011	–0.0748 ± 0.0005	W UMa
	V	0.0172 ± 0.0005	–0.2075 ± 0.0005	–0.0445 ± 0.0006	–0.0690 ± 0.0002	W UMa
	R	0.0152 ± 0.0007	–0.2009 ± 0.0008	–0.0426 ± 0.0008	–0.0655 ± 0.0003	W UMa
V342 Boo	B	0.0383 ± 0.0007	–0.2490 ± 0.0008	–0.0589 ± 0.0007	–0.0931 ± 0.0003	W UMa
	V	0.0375 ± 0.0007	–0.2436 ± 0.0008	–0.0608 ± 0.0008	–0.0898 ± 0.0004	W UMa
	R	0.0341 ± 0.0007	–0.2399 ± 0.0007	–0.0604 ± 0.0007	–0.0875 ± 0.0003	W UMa

OER and LCA are calculated by first defining an "uncertainty function" for each of the integrands (see Appendix B) following the calculus approach of error propogation presented in Hughes and Hase (2010). From this, we obtain the uncertainty of each integrand as a function of phase, which we then integrate to compute the uncertainties of the OER and LCA (Appendices D and E).

Finally, we superpose the two halves of the phase-folded light curves to provide a visual demonstration of the asymmetries in the light curves. We calculate

$$\Delta I(\Phi)_{\text{fit}} = I(\Phi)_{\text{fit}} - I(1-\Phi)_{\text{fit}} \quad (8)$$

and plot this function against Φ ranging from 0 to 0.5. As an example, in Figure 3, we plot $\Delta I(\Phi)_{\text{fit}}$ for the "B" filter for both objects under consideration, and show the difference in the normalized flux at geometrically equivalent points in the orbit of the binary in the bottom panels of each plot. Figure 4 shows just the difference in the normalized flux in all three filters for KID 11405559 and V342 Boo. We note that for both objects, the asymmetry is greatest between the phases 0.15 and 0.25. Also, for the most part, the flux under the secondary half of the phase is greater than that in the primary half. This is consistent with a negative value forΔI and for an OER < 1, as discussed previously. Note also that the magnitude of the asymmetry is marginally greater in V342 Boo than in KID 11405559.

4. Discussion

We have quantified the asymmetries in the light curves of the two objects under consideration: KID 11405559 and V342 Boo. Both systems exhibit a small O'Connell effect, with the asymmetry being the greatest around a phase of about 0.2 (or 0.8). In both systems, ΔI is negative and the OER < 1, which implies that the secondary half of the light curve is brighter than the primary half. It is reasonable to assume that the magnitude and the location of this asymmetry is related, within the starspot model, to the location and characteristics of the starspots on one or the other component of the binary. For a single light curve, phase-folded over one or two orbital cycles of a binary, this information may not be of much consequence. But for EBs in the Kepler and TESS field, where data for several hundred if not several thousand orbital periods are available, this information can prove invaluable in setting constraints or in overruling the starspot model, even without having access to spectroscopic data. For example, we are in the process (Koogler *et al.* in preparation) of analyzing the light curves of several

Table 5. Quantifying the O'Connell Effect in terms of OER and LCA. Please see text (section 3.3) for the definitions of the OER and LCA.

Target	*Filter*	*OER*	*LCA*
KID 11405559	B	0.94 ± 0.02	0.020 ± 0.004
	V	0.94 ± 0.01	0.019 ± 0.002
	R	0.94 ± 0.02	0.018 ± 0.003
V342 Boo	B	0.93 ± 0.01	0.027 ± 0.003
	V	0.93 ± 0.02	0.025 ± 0.004
	R	0.94 ± 0.01	0.022 ± 0.003

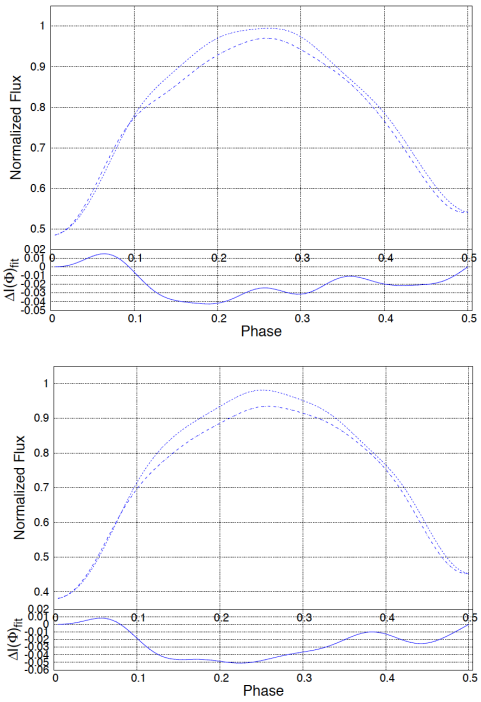

Figure 3. Superposed phased plots of the primary half (dashed line) and the secondary half (dotted line) of the light curves in the B filter for KID 11405559 (upper plot) and V342 Boo (lower plot). The bottom panel (solid blue) shows the difference between the two halves of the light curve. In the absence of any asymmetry, the two curves should coincide, and the solid blue curve in the bottom panel would be a flat line at '0'.

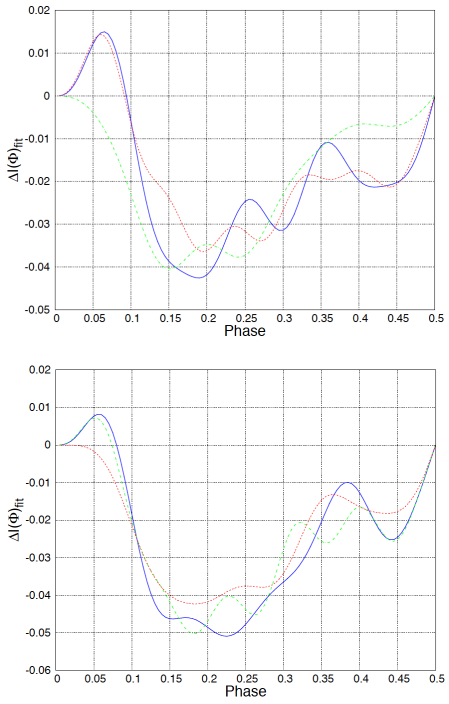

Figure 4. Difference in normalized flux in the B (blue solid curve), V (green dashed), and R (red dotted) filters for KID 11405559 (upper plot) and V342 Boo (lower plot).

hundred EB systems, for which we can analyze hundreds, if not thousands, of consecutive orbits using Kepler data. This gives us information on how the various asymmetry parameters like the OER, LCA, and ΔI evolve in time for hundreds of objects over thousands of orbital cycles. We plan on generating starspot models for a given orbital cycle and propagating this model to fit subsequent orbits in order to test the starspot model. This should enable us to derive constraints on the size, temperature, and lifetimes of the starspots.

5. Acknowledgements

We have made extensive use of the tools available on the AAVSO website (https://www.aavso.org), in particular, the VSP tool to generate star charts, and the VSTAR and VPHOT tools to perform photometry. In addition, we have used the SIMBAD database (http://simbad.u-strasbg.fr/simbad/), operated at CDS, Strasbourg, France, and NASA's Astrophysics Data System. We are thankful for the support provided by the Office of Student Research at Truman State University, and to the Missouri Space Grant Consortium. This research was made possible through the use of the AAVSO Photometric All-Sky Survey (APASS), funded by the Robert Martin Ayers Sciences Fund. The authors would also like to thank the anonymous referee for useful comments and suggestions, which greatly improved the manuscript.

References

Diffraction Limited. 2012, MAXIMDL image processing software (http://www.cyanogen.com).

Gardner, T., Hahs, G., and Gokhale, V. 2015, *J. Amer. Assoc. Var. Star Obs.*, **43**, 186.

Henden, A. A., Templeton, M., Terrell, D., Smith, T. C., Levine, S., and Welch, D. 2016, VizieR Online Data Catalog: AAVSO Photometric All Sky Survey (APASS) DR9, II/336.

Hoffman, D. I., Harrison, T. E., and McNamara, B. J. 2009, *Astron. J.*, **138**, 466.

Høg, E., *et al.* 2000, *Astron. Astrophys.*, **355**, L27.

Hughes, I., and Hase, T. 2010, *Measurements and their Uncertainties: A Practical Guide to Modern Error Analysis*, Oxford University Press, Oxford, 43–44.

Kirk, B. *et al.* 2016, *Astron. J.*, **151**, 68

Koogler, B. R., Shroyer, J. E., and Gokhale, V. M., in preparation.

Kreiner, J. M. 2004, *Acta Astron.*, **54**, 207.

McCartney, S. A. 1999, Ph.D. dissertation, University of Oklahoma.

O'Connell, D. J. K. 1951, *Publ. Riverview Coll. Obs.*, **2**, 85.

Prša, A. 2018, *Modeling and Analysis of Eclipsing Binary Stars, The Theory and Design Principles of PHOEBE*, IOP Publishing, Bristol, U. K.

Prša, A., *et al.* 2011, *Astron. J.*, **141**, 83.

Ricker, G. R., *et al.* 2015, *J. Astron. Telesc. Instrum. Syst.*, **1**, 014003.

Rucinski, S. M. 1973, *Acta Astron.*, **23**, 79.

Rucinski, S. M. 1993, *Publ. Astron. Soc. Pacific*, **105**, 1433.

Rucinski, S. M. 1997, *Astron. J.*, **113**, 407.

Warner, B. D., and Harris, A. W. 2006, *A Practical Guide to Lightcurve Photometry and Analysis*, Springer, New York.

Wilsey N. J., and Beaky M. M. 2009, in *The Society for Astronomical Sciences 28th Annual Symposium on Telescope Science*, The Society for Astronomical Sciences, Rancho Cucamonga, CA, 107.

Wolfram Research Co. 2019, How to Fit Models with Measurement Errors (https://reference.wolfram.com/language/howto/FitModelsWithMeasurementErrors.html).

Appendix A: Obtaining uncertainties on the Fourier coefficients

The uncertainty on each data point is computed as the reciprocal of the signal-to-noise ratio (SNR). Those uncertainties in magnitude are converted into uncertainties in the normalized flux using the formula:

$$I(\Phi)_{\text{obs}} = 10^{-0.4 \times (m(\Phi) - m(\max))}, \quad \text{(A1)}$$

where appropriate.

Using a twelve-term truncated Fourier fit, we use MATHEMATICA's NonlinearModelFit function to run a weighted least squares calculation on our data, weighing each data point by the reciprocal of its uncertainty squared. MATHEMATICA outputs the best estimate, standard error, t-statistic, and p-value for each of the 25 Fourier coefficients. We use the standard error of each Fourier coefficient as its uncertainty in the rest of our uncertainty calculations.

Appendix B: Uncertainty propagation on the Fourier series

The uncertainty δf for a general function f = f (x,y, …) is given by:

$$\delta f = \sqrt{\left(\frac{\partial f}{\partial x}\delta x\right)^2 + \left(\frac{\partial f}{\partial y}\delta y\right)^2 + \ldots}, \quad \text{(B1)}$$

where δx is the uncertainty on x, δy is the uncertainty on y, and so on (Hughes and Hase 2010). Using this, we generate an "uncertainty function" which gives us the uncertainty of the normalized flux as a function of phase.

Now, the Fourier series is given by:

$$I(\Phi) = a_0 + \sum_i a_i \cos(2\pi i\Phi) + \sum_i b_i \sin(2\pi i\Phi)$$

And so,

$$\frac{\partial L}{\partial a_0} = 1, \quad \frac{\partial L}{\partial a_{\text{i}}} = a_i \cos(2\pi i\Phi) + \text{and}, \quad \frac{\partial L}{\partial b_{\text{i}}} = \sin(2\pi i\Phi)$$

Therefore, using Equation B1, the uncertainty on the normalized flux at each phase is given by:

$$\delta I(\Phi) = (\delta a_0)^2 + \sqrt{\sum_i [\delta a_i \cos(2\pi i\Phi]^2 + \sum_i [\delta b_i \sin(2\pi n\Phi)]^2} \quad \text{(B2)}$$

We refer to Equation B2 as the "uncertainty function" in section 3.3.

Appendix C: Uncertainty propagation for ΔI

We calculate ΔI (Fourier) and ΔI (Average) using Equations 4 and 5 (Table 4). ΔI (Fourier) is calculated from the difference in normalized flux between the two maxima from our Fourier fit. We denote the two phases of maxima (one after the primary eclipse and the other after the secondary eclipse) as Φ_p and Φ_s, respectively. We calculate the uncertainty of ΔI (Fourier) by adding δI (Φ_p) and δI (Φ_s) in quadrature, as follows:

$$\delta(\Delta I_{\text{fit}}) = [\delta I(\Phi_p)]^2 + [\delta I(\Phi_s)]^2 \quad \text{(C1)}$$

where δI (Φ_p) and δI (Φ_s) are calculated by using Equation B2.

In order to calculate ΔI (Average), we average data points within ± 0.05 phase of each maxima and then take the difference between the two maxima. The uncertainty on each average is calculated by adding the uncertainties of data points used in quadrature and dividing that by the number of data points:

$$\delta(\langle I_p \rangle) = \frac{\sqrt{(\delta x_1)^2 + (\delta x_2)^2 + \cdots + (\delta x_n)^2}}{n}$$

with a similar expression for δI (Φ_s).

The uncertainty on ΔI (Average) then, is given by adding these uncertainties of the averages in quadrature:

$$\delta(\Delta I_{\text{Ave}}) = [\delta(\langle I_p \rangle)]^2 + [\delta(\langle I_s \rangle)]^2 \quad \text{(C2)}$$

Appendix D: Error propagation for the O'Connell Effect Ratio (OER)

The OER is given by Equation 6:

$$\text{OER} = \frac{\int_{0.0}^{0.5} (I(\Phi)_{\text{fit}} - I(\Phi)_{\text{fit}}) d\Phi}{\int_{0.5}^{1.0} (I(\Phi)_{\text{fit}} - I(\Phi)_{\text{fit}}) d\Phi}$$

From Equation B2,

$$\delta I(\Phi) = (\delta a_0)^2 + \sqrt{\sum_i [\delta a_i \cos(2\pi i\Phi]^2 + \sum_i [\delta b_i \sin(2\pi n\Phi)]^2}$$

And adding δI (Φ) and δI (0.0) in quadrature,

$$\delta(I(\Phi) - I(0.0) = \sqrt{[\delta I(\Phi)]^2 + [\delta I(0.0)]^2} =$$

$$\sqrt{[2(\delta a_0)^2 + \sum_i [\delta a_{\text{i}}]^2 + \sum_i [\delta a_{\text{i}} cos(2\pi i\Phi)]^2 + \sum_i [\delta b_{\text{i}} sin(2\pi i\Phi)]^2}$$

In order to evaluate the errors on the integrals involved in calculating the OER, we make the following approximations:

$$\delta\int_{0.0}^{0.5} [I(\Phi) - I(0.0)] d\Phi \approx \delta\int_{0.0}^{0.5} [\delta(I(\Phi) - I(0.0))] d\Phi, \text{ and}$$

$$\delta\int_{0.5}^{1.0} [I(\Phi) - I(0.0)] d\Phi \approx \delta\int_{0.5}^{1.0} [\delta(I(\Phi) - I(0.0))] d\Phi,$$

and treating $\delta(I(\Phi) - I(0.0))$ as a function of Φ, we integrate over the appropriate limits to obtain the uncertainty for both the numerator and denominator in our expression for the OER.

We then evaluate the uncertainty of the OER, quoted in Table 5, using:

$$\frac{\delta(OER)}{OER} = \sqrt{\left(\frac{\delta\int_{0.0}^{0.5} [I(\Phi) - I(0.0)] d\Phi}{\int_{0.0}^{0.5} [I(\Phi) - I(0.0)] d\Phi}\right)^2 + \left(\frac{\delta\int_{0.5}^{1.0} [I(\Phi) - I(0.0)] d\Phi}{\int_{0.5}^{1.0} [I(\Phi) - I(0.0)] d\Phi}\right)^2} \quad \text{(D1)}$$

Appendix E: Error propagation for the Light Curve Asymmetry (LCA)

The LCA is given by Equation 7:

$$\mathrm{LCA} = \sqrt{\int_{0.0}^{0.5} \frac{(I(\Phi)_{\mathrm{fit}} - I(1.0-\Phi)_{\mathrm{fit}})^2}{I(\Phi)_{\mathrm{fit}}^2}\, d\Phi}$$

The error analysis of the LCA is a bit more involved. For the sake of clarity, let

$$J(\Phi) = I(\Phi) - I(1.0-\Phi),\ K(\Phi)) = \frac{J(\Phi)}{I(\Phi)} \text{ and, } L(\Phi) = [K(\Phi)]^2$$

so that $L(\Phi)$ is the integrand, and we are interested in calculating an expression for $\delta L(\Phi)$.

Note that

$$I(1.0-\Phi) = a_0 + \sum_i a_i \cos[2\pi i(1.0-\Phi)] + \sum_i b_i \sin[2\pi i(1.0-\Phi)].$$

and since,

$$\cos[2\pi\mathrm{i}(1.0-\Phi)] = \cos(2\pi\mathrm{i} - 2\,\mathrm{i}\Phi) = \cos(2\pi\mathrm{i}\Phi) \text{ and,}$$
$$\sin[2\pi\mathrm{i}(1.0-\Phi)] = \sin(2\pi\mathrm{i} - 2\,\mathrm{i}\Phi) = -\sin(2\pi\mathrm{i}\Phi),$$

we have

$$I(1.0-\Phi) = a_0 + \sum_i a_i \cos(2\pi i\Phi) - \sum_i b_i \sin(2\pi i\Phi).$$

Thus,

$$\begin{aligned} J(\Phi) &= I(\Phi) - I(1.0-\Phi) = \\ &= \left[a_0 + \sum_i a_i \cos(2\pi i\Phi) + \sum_i b_i \sin(2\pi i\Phi)\right] \\ &- \left[a_0 + \sum_i a_i \cos(2\pi i\Phi) + \sum_i b_i \sin(2\pi i\Phi)\right] \\ &= 2\sum_i b_i \sin(2\pi i\Phi). \end{aligned}$$

Now, taking the partial derivatives of $L(\Phi)$ with respect to the Fourier coefficients, we get

$$\begin{aligned} \frac{\partial L}{\partial a_0} &= 2K(\Phi)\, J(\Phi)\, [-I(\Phi)^2] \\ &= -2K(\Phi)\, J(\Phi)\, I(\Phi)^2\,. \end{aligned} \tag{E1}$$

$$\begin{aligned} \frac{\partial L}{\partial a_i} &= 2K(\Phi)\, J(\Phi)\, [-I(\Phi)^2] \cos(2\pi i\Phi) \\ &= -2K(\Phi)\, J(\Phi)\, I(\Phi)^2 \cos(2\pi i\Phi), \text{ and} \end{aligned} \tag{E2}$$

$$\begin{aligned} \frac{\partial L}{\partial b_i} &= 2K(\Phi)\left[\frac{2\sin(2\pi i\Phi) - J(\Phi)\sin(2\pi i\Phi)}{I(\Phi)^2}\right] \\ &= \frac{2K(\Phi)\,[2I(\Phi) - J(\Phi)]\sin(2\pi i\Phi)}{I(\Phi)^2}\,. \end{aligned} \tag{E3}$$

And so as before (Hughes and Hase 2010),

$$\delta L(\Phi) = \sqrt{\left(\frac{\partial L}{\partial a_0}\delta a_0\right)^2 + \sum_i \left(\frac{\partial L}{\partial a_i}\delta a_i\right)^2 + \left(\frac{\partial L}{\partial b_i}\delta b_i\right)^2} \tag{E4}$$

where each of the partial derivatives are given by Equations E1, E2, and E3.

Using the same approximation as before, we have:

$$\delta\int_{0.0}^{0.5} L(\Phi)d\Phi \approx \int_{0.0}^{0.5} \delta L(\Phi)d\Phi,$$

We integrate δ L (Φ) over the appropriate limits. We then calculate the uncertainty of the LCA, quoted in Table 5, using:

$$\begin{aligned} \frac{\delta(LCA)}{LCA} &= \frac{1}{2}\left[\frac{\delta\int_{0.0}^{0.5} L(\Phi)\,d\Phi}{\int_{0.0}^{0.5} L(\Phi)\,d\Phi}\right] \\ &\approx \frac{1}{2}\left[\frac{\delta\int_{0.0}^{0.5} L(\Phi)\,d\Phi}{\int_{0.0}^{0.5} L(\Phi)\,d\Phi}\right] \end{aligned} \tag{E5}$$